

<https://doi.org/10.1038/s40494-026-02476-w>

# Identification of key areas for soil conservation service and driving factors under ecological restoration projects in South China Karst

Check for updates

Yating Mu<sup>1</sup>, Kangning Xiong<sup>1</sup> ✉, Xiaoyu Yan<sup>1</sup>, Guohua Liu<sup>2</sup> & Lulu Cai<sup>1,3</sup>

It is urgent and challenging to evaluate the effects of soil conservation (SC) under ecological restoration projects (ERPs) in karst regions. In this study, the surrogate biophysical method was adopted to investigate the spatiotemporal evolution of SC under ERPs in Guizhou Province from 2000 to 2023. We found that SC showed an increasing trend, and SC hotspots were mainly spatially aggregated in southern Guizhou Province (Qianxinan and Qiannan), while its cold spots were concentrated primarily in the western and northern regions. Returning farmland to forest (RFTF) exhibited the strongest SC effectiveness. However, returning farmland to water bodies (RFTW) became increasingly effective in enhancing SC over the study period (0.01–0.04). This indicates that RFTW showed potential for further enhancing SC in karst regions. The dominant factors of SC demonstrated temporal variability, and precipitation, slope, and soil types were the dominant factors of SC in Guizhou Province during the study period.

China's high population density and significant economic and social needs have resulted in the adoption of unsustainable land management practices over the long term<sup>1</sup>. Alterations in the spatial distribution of land use will have a direct impact on the ecosystem's structure, function, and dynamics<sup>2–4</sup>. The study of land-use management and its impact on the environment is becoming a prominent field in the realm of global environmental change<sup>5</sup>. As the demand for land grows, it is essential for policymakers to track changes in land use and their effects. This forms the foundation for carrying out extensive ecological restoration projects (ERPs). Previous studies have demonstrated that using ERPs can enhance ecosystem services (ESs)<sup>6</sup>, and the Grain-for-Green Project (GFGP) in Shaanxi Province was found to significantly reduce soil erosion, benefiting soil conservation (SC) efforts<sup>7</sup>. However, any single or centralized land use strategy for various biota could lead to undesirable consequences. Even though the national government has put in place ERPs, not all the areas targeted may have experienced significant soil erosion. As a result, the ESs have not been greatly enhanced even with ERPs<sup>8</sup>. To determine optimal ecological restoration pathways, it is crucial to evaluate the contribution of different ERPs and plan for effective land management. SC refers to the ability of ecosystems to prevent soil erosion and store sediments. It prevents land degradation and flood disasters by

regulating the environment and is one of the most crucial services provided by terrestrial ecosystems<sup>9</sup>. The quantification of SC is increasingly recognized as key in the aforementioned research fields. Providing spatially explicit information on key areas of SC is crucial for developing effective ERPs, this allows for the identification of areas that offer high-value services and the implementation of targeted management strategies<sup>10–12</sup>.

Karst areas are among the world's major ecologically fragile regions, accounting for approximately 20% of the global land area<sup>13</sup>. As the world's largest karst ecosystem, the South China Karst, due to its intricate geological settings, extensive karst activities, and unreasonable land use patterns, has suffered severe soil erosion, eventually leading to rocky desertification and further exacerbating regional poverty<sup>14–16</sup>. Since the 1980s, the government has initiated ERPs to address soil erosion and rocky desertification in karst regions<sup>17</sup>. At present, the trend of rocky desertification development has been reversed in the context of ERP implementation<sup>18</sup>. However, it still faces challenges such as effectively maintaining treatment results and increasing treatment difficulty. Studies have shown that karst ecological restoration has great potential in improving biodiversity and providing ecosystem services, but restoration outcomes depend on environmental conditions<sup>19</sup>. Furthermore, ecological projects typically exhibit a threshold effect on enhancing

<sup>1</sup>School of Karst Science, Guizhou Normal University/State Engineering Technology Institute for Karst Desertification Control, Guiyang, China. <sup>2</sup>State Key Laboratory of Urban and Regional Ecology, Research Center for Eco-Environmental Sciences, Chinese Academy of Sciences, Beijing, China. <sup>3</sup>Institute of Geographic Sciences and Natural Resources Research, Chinese Academy of Sciences, Beijing, China. ✉e-mail: [xiongkn@163.com](mailto:xiongkn@163.com)

SC capacity<sup>20</sup>. Hence, clarifying the SC capacity of different ERPs is essential to maximizing the effectiveness of ecological projects. Current research on soil conservation services in karst areas mainly covers topics such as spatio-temporal variations of soil conservation<sup>21,22</sup>, trade-offs/synergies between soil conservation and other services<sup>12,21,23</sup>, driving factors and their scale effects<sup>24–26</sup>, and has achieved significant results. However, research on the soil conservation effects of different ERPs in karst areas and their driving mechanisms for SC is still relatively scarce. Therefore, in order to quantify and consolidate the effect of rocky desertification control, it is necessary to explore the changes in SC after the implementation of ERPs in karst areas and the influence of environmental factors on its spatio-temporal distribution.

At present, spatial mapping of soil erosion in terrestrial ecosystems is mainly based on empirical soil erosion models (such as the RUSLE model)<sup>27–29</sup>. Based on empirical models, SC is quantified as the difference between the actual soil loss and potential soil loss under different land uses<sup>30</sup>. However, the parameters of empirical SC models are based on small-scale spatial field observation data, which have drawbacks such as difficulty in obtaining parameters and complex calculations. Moreover, when conducting evaluations at a large spatial scale, the model parameters must be simplified, which may lead to uncertainties in the SC assessment results<sup>31</sup>. Net primary productivity (NPP) serves as a key indicator of ecosystem functioning, and has been demonstrated to be linked to the overall value of ecosystems<sup>32</sup>. Research has demonstrated a positive relationship between NPP and the provision of various supporting and regulating ESs<sup>33</sup>. Hence, researchers have proposed several biophysical methods to attain more objective and consistent evaluations. For instance, the concept of solar energy has been introduced as a common currency for ES assessments<sup>34</sup>. Some studies have assumed a spatial correlation between ESs and NPP, using NPP as a parameter to delineate the boundaries of biodiversity conservation areas in the United States<sup>35</sup>. Additionally, environmental variables such as biomass, precipitation, temperature, and elevation have been employed to map the spatial distribution of five ESs in South Africa<sup>36</sup>. The biophysical proxy method has been applied for ES valuation in Argentina<sup>37,38</sup>. Subsequently, the NPP method was modified to enhance its applicability in ES assessment in China, with comparisons made between the NPP method and the RUSLE method to assess SC services in Jiangxi Province<sup>39,40</sup>. The findings further support the feasibility and convenience of the NPP method. All the aforementioned methods involve incorporating NPP parameters into the model, modeling NPP using Normalized Difference Vegetation Index (NDVI) data and various environmental factors to produce straightforward but causal estimates of ESs. This means that the NPP modeling approach can also be directly connected to the spatio-temporal distribution of SC.

NPP directly reflects the capacity of vegetation to intercept rainfall, consolidate soil via root systems, and reduce surface runoff, thereby driving improvements in SC. In turn, SC promotes increases in NPP through nutrient retention<sup>23</sup>. Consequently, a generally positive correlation exists between NPP and SC. Karst ecosystems exhibit distinctive characteristics, including rocky desertification, shallow soil layers, exposed bedrock, and a dual-layer hydrological structure<sup>41,42</sup>. Taking the Maolan Karst Stone Forest as an example, as a typical representative of the “dense forest–shallow soil” habitat in karst regions, the relationship between its NPP and SC follows the general patterns observed across karst areas. However, the high habitat heterogeneity of karst ecosystems results in regional variations in the correlation between NPP and soil conservation. Owing to the complex terrain, fragile ecology, and slow soil formation rate in karst regions, traditional models struggle to accurately quantify the impact of the rocky desertification process on soil conservation functions<sup>25</sup>. Compared with non-karst areas, the unique binary three-dimensional structure (aboveground and underground karst features) of karst areas limits the applicability of traditional RUSLE model parameters (such as rainfall erosivity factor and soil erodibility factor) in karst areas<sup>25,43</sup>. Furthermore, the South China Karst accounts for approximately 5% of the global growth in biomass and has seen the most significant rise in forest area and carbon storage on a global scale<sup>44</sup>. The NPP

modeling approach allows for the prioritization of various ecological restoration strategies by pinpointing crucial SC areas and clarifying the ecological impacts of ecological restoration initiatives<sup>40</sup>. Importantly, compared with traditional methods, the NPP proxy indicator approach is simpler for studies at large scales and can directly reflect the distribution of key SC service areas without the need to use more complex modeling methods that may yield specific numbers of SC<sup>40</sup>. Therefore, this study adopted the NPP proxy index method to evaluate the spatio-temporal evolution of SC in Guizhou Province, identify its key areas, further reveal the SC benefits of different ERPs, and clarify the driving mechanisms underlying the spatial distribution of SC.

This study is based on multi-source spatiotemporal data, such as meteorological, soil, and remote sensing image data. The biophysical proxy method was used to reveal the relative changes in SC services instead of employing more intricate modeling techniques to determine the exact quantity of SC. The specific objectives of this study were to: (1) clarify the spatio-temporal evolution characteristics of SC in karst areas; (2) reveal the correlation between the spatial distribution of SC and different environmental factors; (3) explore effective strategies for improving the SC capacity in karst areas in the future by comparing SC effectiveness under different ERPs. The findings strongly support the promotion of karst desertification control and sustainable ecosystem management in karst regions.

## Methods

### Study area

Guizhou Province is situated in the center of South China Karst (24°37′–29°13′N, 103°36′–109°35′E) (Fig. 1), and soil and water conservation, as well as the desertification control in karst ecosystems, are highly typical and representative<sup>45</sup>. The climate is characterized as a subtropical humid monsoon climate, with annual average temperatures ranging from 14°C to 16°C and average annual precipitation between 1100 and 1300 mm. The vegetation type is mainly subtropical evergreen deciduous broad-leaved mixed forest. The soil is predominantly composed of yellow loam and lime soil. The land reclamation rate in the province is double the national average, and its poor land-use planning has resulted in severe karst desertification. In 2000, Guizhou Province launched the Grain for Green Program (GFGP). Since 2008, the province has continuously implemented comprehensive karst desertification control projects, including the construction and protection of forest and grass vegetation, the development of herbivorous animal husbandry, and the construction of small-scale water conservancy and soil and water conservation facilities. In 2023, the karst area in the province was 109,084 km<sup>2</sup>, accounting for 61.90% of the total land area of Guizhou. Among them, the karst desertification area was 15,514 km<sup>2</sup>, accounting for 8.80% of the total land area of Guizhou. In recent years, remarkable achievements have been made in karst desertification control through the implementation of ecological restoration measures.

### Data sources

Meteorological data (including precipitation, temperature, and radiation data) were retrieved from the China Meteorological Data Sharing Service System (Table 1). The Co-kriging interpolation method was adopted to perform spatial interpolation of the meteorological data for the study area. Soil data (including soil types, texture, and soil organic carbon content) were obtained from the 1:1,000,000 scale soil map of China from the Second National Soil Survey. The map was first clipped to the study area of Guizhou Province, and the corresponding soil physicochemical parameters were assigned to each soil type vector unit according to the attached attribute database of the soil census. Digital elevation model (DEM) datasets with a resolution of 90 m were downloaded from the US Geological Survey (USGS). Following preprocessing involving clipping and sink filling, the slope factor was extracted using ArcGIS software. NDVI data were acquired from the NASA EOS Data Gateway, with a series of preprocessing steps including radiometric calibration, atmospheric correction, cloud masking, and topographic correction conducted in ENVI and ArcGIS. The land-use type classification data were obtained from the Resource and Environmental

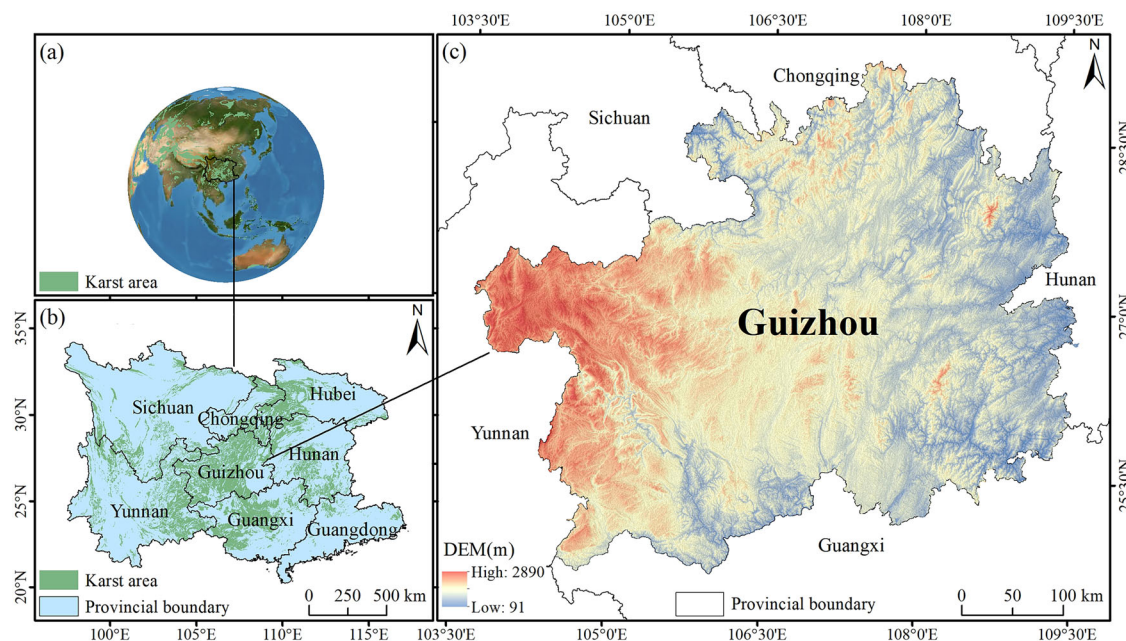


Fig. 1 | Location of the study area. a Karst distribution area in the Eastern Hemisphere, b South China Karst, c Study area.

Table 1 | Datasets and resources used in this study

Data type	Resolution	Unit	Data sources
DEM	90	m	<a href="https://gdex.cr.usgs.gov/gdex/">https://gdex.cr.usgs.gov/gdex/</a>
MODIS NDVI	250	m	<a href="https://ladsweb.nascom.nasa.gov/data/">https://ladsweb.nascom.nasa.gov/data/</a>
Soil data	1000	m	<a href="https://www.resdc.cn">https://www.resdc.cn</a>
Land use	250	m	<a href="https://www.resdc.cn/">https://www.resdc.cn/</a>
Meteorological data			<a href="http://cdc.cma.gov.cn">http://cdc.cma.gov.cn</a>
Vegetation types	1000	m	<a href="http://www.ncdc.ac.cn">http://www.ncdc.ac.cn</a>
Nighttime light index	1000	m	<a href="http://www.geodata.cn">http://www.geodata.cn</a>
Administrative boundary			<a href="https://www.gscloud.cn/">https://www.gscloud.cn/</a>

Table 2 | Correctional coefficient for different degrees of rocky desertification

	NKRD	PKRD	LKRD	MKRD	HKRD	SKRD
$\alpha$	0.10	0.25	0.40	0.60	0.80	0.95

NKRD Non-karst rocky desertification, PKRD potential karst rocky desertification, LKRD light karst rocky desertification, MKRD moderate karst rocky desertification, HKRD high karst rocky desertification, SKRD severe karst rocky desertification.

Science Data Platform, Institute of Geographic Sciences and Natural Resources Research, CAS. The land use types in Guizhou Province were classified into farmland, forest, grassland, water bodies, construction land, and unutilized land. Vegetation type data were obtained from the National Cryosphere Desert Data Center. Nighttime light data were acquired from the National Earth System Science Data Center. Finally, the aforementioned datasets were cropped and projected to a unified coordinate system within the ArcGIS platform based on the administrative boundaries of Guizhou Province and resampled to a 250 m resolution.

### Land use transition

To reveal the mutual transformation relationships among different land use types across various time points, a land-use transfer matrix was employed

for quantitative analysis. This matrix reflects the system state and provides a quantitative description of state transitions<sup>46</sup>, with its calculation formula presented as follows:

$$S_{ij} = \begin{bmatrix} S_{11} & \cdots & S_{1n} \\ \vdots & \ddots & \vdots \\ S_{n1} & \cdots & S_{nn} \end{bmatrix} \quad (1)$$

Where  $S_{ij}$  represents the area of land use type  $i$  at the beginning of the study period converted to land use type  $j$  at the end of the study period, and  $n$  represents the total number of land use types.

### Surrogate model

The biophysical proxy model uses NPP as the core indicator to assess ES values. This method involves significantly fewer parameters and facilitates the assessment of dynamic changes at large scales<sup>37</sup>. Nonetheless, this approach is tailored to specific regions and requires adjustments to be applicable in different locations. Zhang et al.<sup>39</sup>, mapped the spatial pattern of SC in China’s ecological regions using environmental variables such as biomass and its stability, soil erodibility, and slope. They assumed that the SC capacity of an ecosystem is relatively high when the biomass is sufficient, soil erodibility is low, and slopes are gentle. Since rocky desertification is widespread in karst areas, this study incorporates a rocky desertification factor to modify the model to make the SC assessment in karst areas more realistic. Previous studies have established the model based on the causal relationship between environmental variables and SC. Therefore, the model equation modified according to the relationship between rocky desertification and SC is as follows.

$$SC = NPP \times (1 - VC_{npp}) \times (1 - K) \times (1 - F_{slo}) \times (1 - \alpha) \quad (2)$$

Where SC denotes the relative capacity of soil conservation services (dimensionless). NPP is the sum of the annual net primary production of vegetation.  $VC_{npp}$  represents the standard deviation of NPP over a year, and  $K$  is the soil erodibility factor, calculated using the EPIC equation (Eq. 4).  $F_{slo}$  is the surface slope,  $\alpha$  is the rocky desertification factor, with reference to Gao and Wang<sup>47</sup> (Table 2). According to previous NPP modeling approaches, all

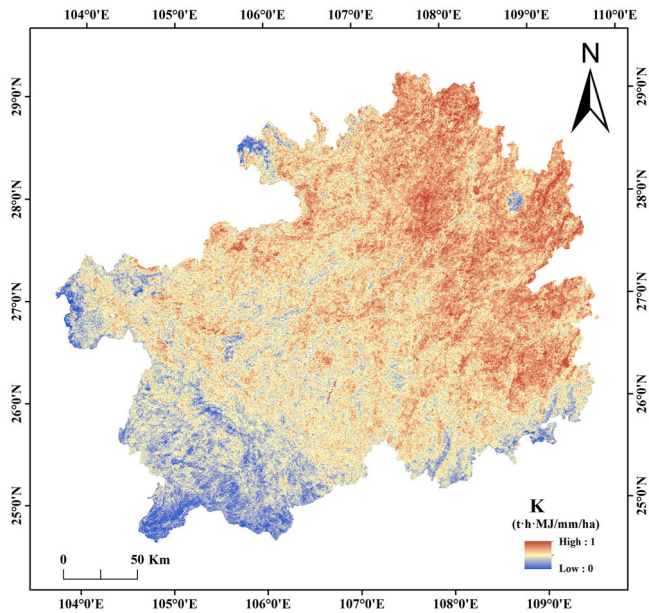


**Fig. 2 | Spatial distribution of the soil erodibility factor (K).** Spatial pattern of soil erodibility (*K*, unit: t·h·MJ/mm/ha). Color gradient from blue (*K*=0, low) to red (*K*=1, high) indicates erodibility magnitude.

**Table 3 | Classification standards for rocky desertification degrees**

Rocky desertification degrees	NDVI (%)	Rock exposure rate (%)
NKRD	>70	<40
PKRD	50–70	>40
LKRD	35–50	>60
MKRD	20–35	>70
HKRD	10–20	>80
SKRD	<10	>90

NKRD Non-karst rocky desertification, PKRD potential karst rocky desertification, LKRD light karst rocky desertification, MKRD moderate karst rocky desertification, HKRD high karst rocky desertification, SKRD severe karst rocky desertification.

parameters need to be normalized so that the relative capacity of SC falls between 0 and 1.

The surrogate biophysical model developed in this study integrates dynamic vegetation changes, soil physicochemical properties, topographic conditions, and karst-specific rocky desertification factors. It is generally consistent with the ecological context of Guizhou Province, where karst desertification and vegetation degradation are the primary drivers of soil erosion. Mechanistically, the model helps to characterize the ecological processes underlying soil conservation. Importantly, the introduction of a rocky desertification correction factor may help overcome key limitations of the empirical RUSLE model in adapting to the unique erosion mechanisms in karst bare rock areas. In addition, the surrogate biophysical model can improve the comparability of assessment results across spatially heterogeneous karst landforms by evaluating the relative soil conservation capacity. The model shows potential advantages for evaluating the effectiveness of ERPs on a large spatial scale and for spatial prioritization in conservation planning.

NPP was estimated using the terrestrial Carnegie-Ames-Stanford Approach (CASA) model<sup>48</sup>, with the following formula:

$$NPP(x, t) = APAR(x, t) \times \epsilon(x, t) \quad (3)$$

Where  $NPP(x, t)$  ( $g\ C\ m^{-2}\ yr^{-1}$ ) denotes the net primary production rate at location  $x$  at time  $t$ ,  $APAR(x, t)$  ( $MJ\ m^{-2}\ s^{-1}$ ) refers to the photosynthetically active radiation absorption rate at location  $x$  at time  $t$ , and the parameter  $\epsilon(x, t)$  ( $g\ C\ MJ^{-1}$ ) denotes the light-use efficiency of the vegetation at location  $x$  at time  $t$ . The annual total NPP ( $g\ C\ m^{-2}\ yr^{-1}$ ) is the sum of monthly NPP values over 12 months. The CASA model requires land use, NDVI, and meteorological data as inputs.

Soil erodibility factor ( $K$ ) reflects the sensitivity of the soil to the erosive power of rainfall. The  $K$  value was calculated using the EPIC model<sup>49</sup>, as shown in Fig. 2.

$$K = 0.1317 \left\{ 0.2 + 0.3 \exp \left[ 0.0256SAN \left( 1 - \frac{SIL}{100} \right) \right] \right\} \times \left( \frac{SIL}{CLA + SIL} \right)^{0.3} \times \left( 1 - \frac{0.25C}{C + \exp(3.72 - 2.95C)} \right) \times \left( 1 - \frac{0.7SNI}{(1 - SNI) + \exp(22.9SNI - 5.51)} \right) \quad (4)$$

Where SAN represents the sand content (>0.05 mm), %; SIL represents the silt content (0.002–0.05 mm), %; CLA represents the clay content (<0.002 mm), %; SNI = 1-SAN/100; and C represents the content of soil organic carbon, %. The value 0.1317 is the conversion factor for  $K$  from US units to international standard metric units ( $t\ h\ MJ^{-1}\ mm^{-1}\ ha^{-1}$ ).

### Classification of rocky desertification degree

The essence of rocky desertification in Guizhou Province lies in the coupling process of vegetation cover degradation and intensified bedrock exposure<sup>15</sup>. Therefore, this study adopted the dual indicators of NDVI and bedrock exposure rate as the classification standard for rocky desertification, which is highly compatible with the core characteristics of rocky desertification in the karst areas of Guizhou Province and consistent with the vegetation-bedrock gradient pattern of Guizhou’s karst landforms (i.e., decreasing vegetation cover and increasing bedrock exposure). In this study, rocky desertification grades were classified with reference to the research of Zhang et al.<sup>50</sup> and Xi et al.<sup>45</sup> on the karst areas of Guizhou Province (Table 3).

### Gi\* statistics-based hotspots and coldspots analysis

The Getis-Ord  $G_i^*$  statistic in spatial analysis was calculated using ArcGIS. Distance-based spatial weights were constructed to calculate the clustering index ( $G_i^*$ ) and its significance Z-value for each analysis unit. Based on Z-values of  $\pm 1.65$ ,  $\pm 1.96$ , and  $\pm 2.58$ , which correspond to confidence levels of 90%, 95%, and 99%, respectively—areas were classified as hot (cold), hotter (colder), and extremely hot (extremely cold) spots. This classification revealed the spatial clustering of SC capacity, facilitating the identification of priority management areas.

### Geographical detector

The Geographical Detector is a statistical method designed to detect spatial heterogeneity and identify driving factors<sup>51</sup>. In this study, we employed the Factor Detector to examine the relationships between SC and various driving factors (elevation, soil types, vegetation types, slope, land use types, precipitation, fractional vegetation coverage (FVC), and nighttime light index (NLI)), thereby further analyzing the driving mechanisms of SC. The  $q$ -statistic is used to quantify the degree of influence of driving factors  $X$  on the spatial differentiation of variable  $Y$ <sup>52</sup>:

$$q = 1 - \frac{\sum_{h=1}^L N_h \sigma_h^2}{N \sigma^2} \quad (5)$$

where  $h = 1, \dots, L$  denotes the stratification of  $Y$  or  $X$ ;  $N_h$  and  $N$  represent the number of units in layer  $h$  and the entire study area, respectively;  $\sigma_h^2$  and  $\sigma^2$  are the variances of layer  $h$  and the entire study area, respectively; and  $q \in [0, 1]$ .

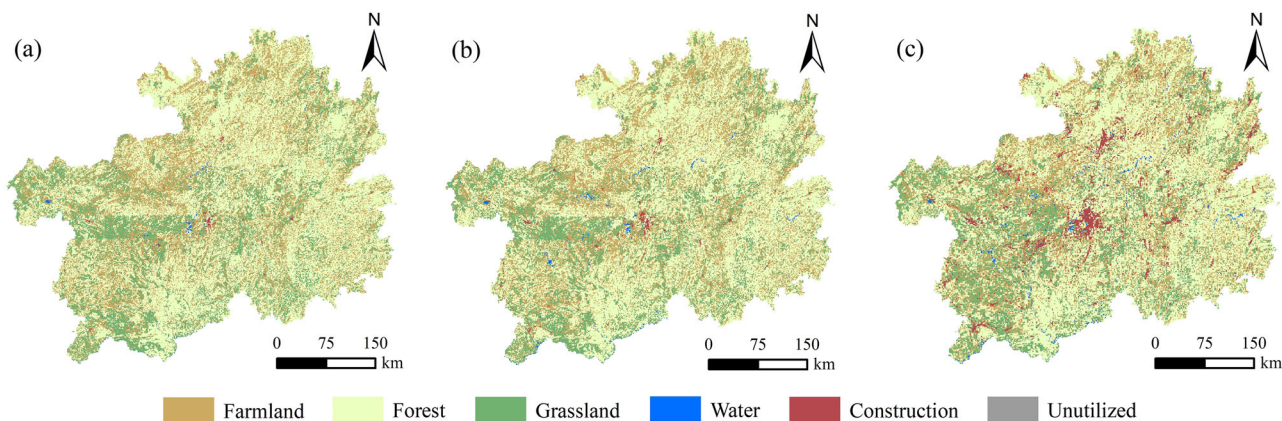


Fig. 3 | Spatial distribution of land uses in Guizhou province. a 2000, b 2013, c 2023.

Table 4 | Changes in land use types from 2000 to 2023

Land uses	Area (km <sup>2</sup> )			Area change (km <sup>2</sup> )		
	2000	2013	2023	2000–2013	2013–2023	2000–2023
Farmland	49314.92	49153.32	45482	-161.60	-3671.32	-3832.92
Forest	93343.44	94741.14	90962.08	1397.70	-3779.06	-2381.36
Grassland	31654.75	29512.44	29975.12	-2142.31	462.68	-1679.63
Water bodies	382.16	662.19	1127.18	280.03	464.99	745.02
Construction land	638.81	1279.92	8151.60	641.11	6871.68	7512.79
Unutilized	37.99	23.06	28.36	-14.93	5.30	-9.63

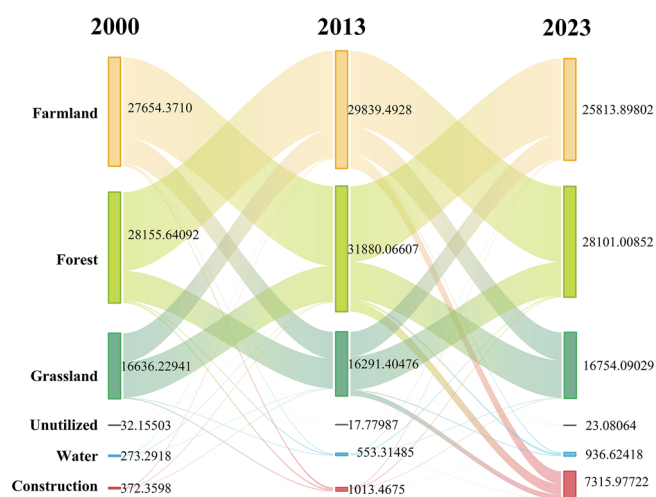


Fig. 4 | Land use type transfer Sankey diagram from 2000 to 2023. Vertical bars represent six land use types with labeled areas. Flow band width indicates the magnitude of area transfer, and different colors distinguish land use categories.

## Results

### Land use change pattern

Land use types were dominated by forest, followed by farmland and grassland, with both water bodies and unutilized land accounting for less than 1%. The central region was mostly construction land, while grasslands were primarily located in the western region of Guizhou Province (Fig. 3). All land use types showed a decreasing trend except for construction land and water bodies from 2000 to 2023 (Table 4). The areas of forest, water bodies, and construction land increased by 1397.70, 280.03, and 641.11 km<sup>2</sup> from 2000 to 2013, respectively; while farmland, grassland, and unutilized

land showed a decreasing trend. Compared to the previous period, construction land significantly increased by 6871.68 km<sup>2</sup>, while forest experienced the most significant decrease (-3779.06 km<sup>2</sup>) from 2013 to 2023.

The transfer of land use types between 2000 and 2023 was primarily dominated by exchanges among farmland, forest, and grassland, with forest exhibiting the largest transfer area and unutilized land the least (Fig. 4). During the 2000–2013 period, the largest transfer was from farmland to forest, accounting for 68.43% of the area transferred to forest and 73.13% of the area transferred from farmland (Table 5). Newly added construction land and water bodies in 2013 were primarily converted from forest, farmland, and grassland in 2013. The pattern of land use transformation between 2013 and 2023 was similar to that of the previous period, with a smaller area of farmland converted to forest and grassland compared to 2000–2013. In contrast, the areas converted from farmland, forest, and grassland to construction land were significantly larger than those in the previous period, with 3,294.65 km<sup>2</sup>, 2,642.33 km<sup>2</sup>, and 1,348.97 km<sup>2</sup> being converted, respectively (Table 6).

### Spatio-temporal distribution of SC

The mean SC values in 2000, 2013, and 2023 were 0.19, 0.23, and 0.26, respectively, showing an increasing trend and significant spatial heterogeneity, with generally higher values in the southern regions compared to the northern and northwestern regions of Guizhou Province (Fig. 5). In 2000, high-value SC areas were primarily distributed in the southern part, particularly in Qianxinan, Qiannan, and Qiandongnan, while the low-value areas were mostly located in Bijie, Zunyi, Tongren, and Guiyang in 2000, and by 2013, the regions with low SC had improved (Fig. 6). By 2023, high-value SC areas had expanded, mainly in Qianxinan, Qiannan, Liupanshui, Anshun, and Bijie, while low-value SC areas were primarily found in Guiyang, Zunyi, Tongren, and Qiandongnan. Overall, the spatial distribution of SC varied over time. Although Zunyi, Tongren, and Guiyang had improved SC, they remained in low-value SC areas.

Forests had the highest mean SC values in 2000 and 2013, with values of 0.20 and 0.24, respectively. In 2023, the mean SC value of forests (0.26)

**Table 5 | Transfer matrix of land uses in Guizhou province from 2000 to 2013**

2013 2000	Construction land	Farmland	Forest	Grassland	Unutilized	Water bodies
Construction land	266.45	162.94	132.82	71.51	0	5.09
Farmland	476.89	21660.55	20223.33	6763.58	3.43	187.13
Forest	325.16	19980.84	65187.80	7588.78	7.34	253.52
Grassland	205.03	7261.38	9055.80	15018.52	6.46	107.57
Unutilized	0.77	6.74	15.80	8.84	5.83	0
Water bodies	5.62	80.89	125.59	61.20	0	108.87

**Table 6 | Transfer matrix of land uses in Guizhou province from 2013 to 2023**

2023 2013	Construction land	Farmland	Forest	Grassland	Unutilized	Water bodies
Construction land	835.62	161.40	187.80	80.91	0.62	13.58
Farmland	3294.65	19313.83	19185.74	7084.88	4.94	269.29
Forest	2642.33	19268.74	62861.07	9492.95	9.97	466.07
Grassland	1348.97	6255.48	8492.21	13221.03	7.55	187.19
Unutilized	2.50	1.78	10.71	2.28	5.28	0.50
Water bodies	27.52	126.50	224.55	93.07	0	190.55

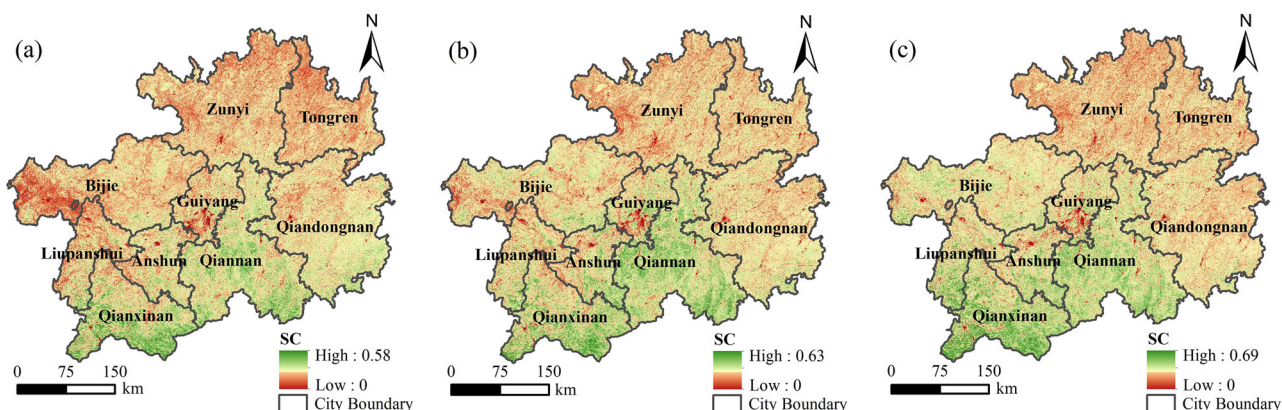


**Fig. 5 | Spatial distribution of SC in Guizhou province. a 2000, b 2013, c 2023.**

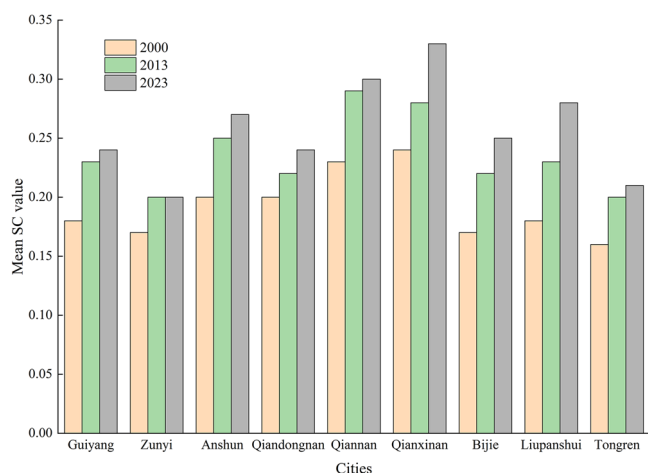


**Fig. 6 | The mean SC values of different cities in Guizhou Province in 2000, 2013, and 2023. Bar chart of mean SC values for nine cities in Guizhou Province.**

was second only to that of grasslands (0.27). Construction land had the lowest mean SC values during the 2000–2023 period in Guizhou province (Fig. 7a). The combined SC of grasslands and forests accounted for 73% of the total SC of all land uses. However, the total SC of water bodies, construction land, and unutilized land each accounted for less than 1% of the total SC in Guizhou province. It is evident that forests and grasslands are the main contributors to soil conservation.

As the slope increased, the total SC showed a trend of decreasing first, then increasing, and finally decreasing, while the mean SC showed the opposite trend of increasing first, then decreasing, and finally increasing (Fig. 7b). The total SC peaked at a slope of 8–15° (160028.25), while the mean SC was highest between 5 and 8° (0.27). The total SC first increased and then decreased with altitude, reaching the highest value in the 500–1000 m altitude region (1968.30) (Fig. 7c). The mean SC did not vary significantly with altitude and was lowest at altitudes above 2000 m (0.19).

In Guizhou Province, both the mean and total SC initially increased and then decreased with increasing precipitation (Fig. 7d). The mean SC was highest in the 1100–1200 mm range of precipitation (0.27), while the total SC peaked at 268,283.83 in the 1000–1100 mm range. Taking the 1100–1200 mm precipitation interval as the threshold, the total SC in 2000

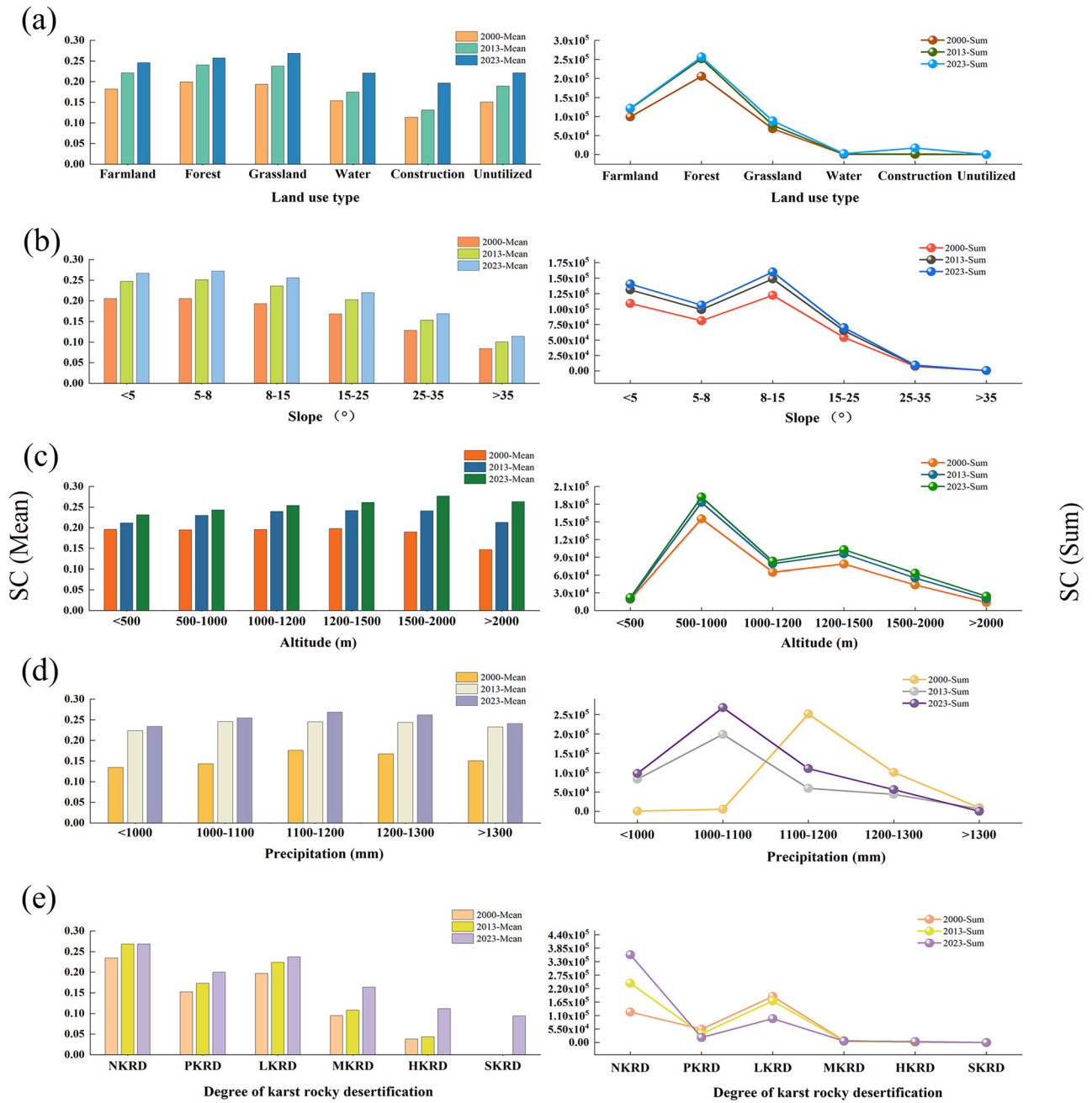


Fig. 7 | SC under different environmental conditions in 2000, 2013, and 2023. a Land use type, b Slope, c Altitude, d Precipitation, e Degree of karst rocky desertification.

was lower than that in other years below this threshold, but higher than that in other years above this threshold.

The trends of mean and total SC were consistent: as the degree of rocky desertification deepened, both showed a trend of decreasing first, then increasing, and finally decreasing (Fig. 7e). The mean and total SC were the highest in non-karst rocky desertification (NKRD) areas at 0.27 and 358526.35, respectively; while they were the lowest in severe karst rocky desertification (SKRD) areas, both being 0. However, the mean SC in light karst rocky desertification (LKRD) (0.22) was higher than that in potential karst rocky desertification (PKRD) (0.17). In terms of temporal changes, the mean SC for all degrees of rocky desertification during the period 2000–2023 showed an increasing trend. However, the total SC of PKRD and LKRD areas in 2023 was lower than that in 2000 and 2013.

### Hotspots and coldspots of SC

The statistically significant hotspots and coldspots at different confidence levels are presented in Fig. 8. From 2000 to 2023, SC hotspots were predominantly distributed in the southern regions of Guizhou Province, whereas coldspots were concentrated in the northern and northwestern regions (Fig. 8). In 2000, SC hotspots clustered in Qianxinan, southern Qiannan, and southern Qiandongnan, while coldspots were mainly located in northwestern Zunyi, Tongren, and western Bijie. By 2013, the hotspot coverage in Qiandongnan exhibited a discernible contraction, whereas the coldspot areas in the north expanded toward the northeast (Fig. 8b). In 2023, the southern hotspots shrank further, accompanied by a marked expansion of northern coldspots.

The statistically significant hotspots of SC accounted for 23.49, 23.02, and 23.75% of Guizhou Province’s total area in 2000, 2013, and 2023,

**Fig. 8 | Hot and cold spot analysis of SC in Guizhou Province. a 2000, b 2013, c 2023.**

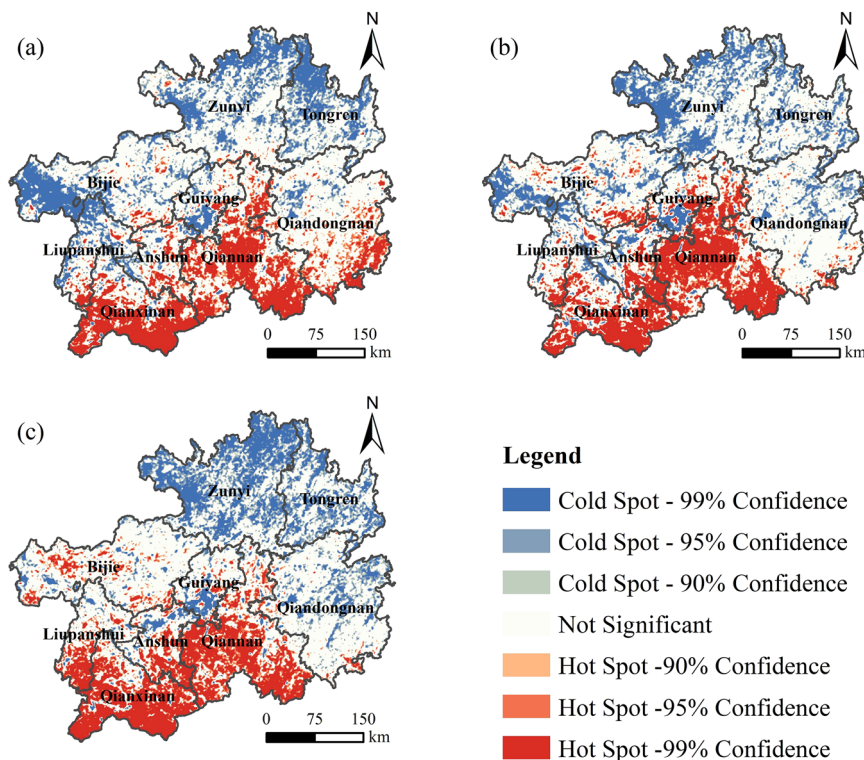


**Table 7 | Statistics on the hotspots and coldspots of SC in Guizhou Province**

	2000		2013		2023	
	Mean SC value	Area percentage (%)	Mean SC value	Area percentage (%)	Mean SC value	Area percentage (%)
Cold spots-99%	0.12	13.43	0.15	11.92	0.17	12.47
Cold spots-95%	0.15	7.91	0.18	8.29	0.20	8.98
Cold spots-90%	0.16	4.81	0.19	5.36	0.21	5.54
Not significant	0.19	50.65	0.23	51.41	0.25	49.26
Hot spots-90%	0.23	3.20	0.27	2.63	0.29	2.81
Hot spots-95%	0.24	5.16	0.28	4.37	0.30	4.86
Hot spots-99%	0.27	14.83	0.32	16.02	0.35	16.08

**Table 8 | Changes in SC under different ERPs during 2000–2023**

ERPs	2000–2013			2013–2023		
	Area (km <sup>2</sup> )	Mean	Sum	Area (km <sup>2</sup> )	Mean	Sum
CFTC	476.89	-0.00151	-7.87	3290.65	0.01	345.71
RFTF	20223.33	0.04	9135.25	19184.74	0.02	3631.16
RFTG	6763.58	0.04	3175.81	7084.88	0.03	2268.13
RFTU	3.43	0.03	1.27	4.94	0.02	0.87
RFTW	187.13	0.01	18.72	269.07	0.04	107.26
CGTF	9055.80	0.04	4470.87	8491.21	0.02	2216.11

RFTF returning farmland to forest, RFTG returning farmland to grassland, CFTC converting farmland to construction land, RFTW returning farmland to water bodies, RFTU returning farmland to unutilized land, CGTF converting grassland to forest.

respectively (Table 7); the corresponding area proportions of coldspots stood at 26.15, 25.57, and 26.99% over the same period. The annual mean SC values of the hotspots were in the ranges of 0.23–0.27, 0.27–0.32, and

0.29–0.35 in 2000, 2013, and 2023, while those of the coldspots were 0.12–0.16, 0.15–0.19, and 0.17–0.21, respectively. The above results indicate that the hotspots exhibit the highest SC capacity.

**Changes in SC under different ERPs**

Based on the analysis results of land use type transfer, six ERP types were selected to explore the changes in SC under different ERPs in Guizhou province during 2000–2023 (Table 8). Returning farmland to forest (RFTF) was the primary driver of the increase in total SC, significantly surpassing other ERPs. The increase in SC attributed to RFTF accounted for approximately 42.3–54.37% of the total increase. This was then followed by converting grassland to forest (CGTF) and returning farmland to grassland (RFTG), which together accounted for approximately 45.51–52.33% of the total increase. Converting farmland to construction land (CFTC) resulted in a slight reduction in mean and total SC between 2000 and 2013 (–0.00151, –7.87), and an increase in the total SC (345.71) from 2013 to 2023. Returning farmland to water bodies (RFTW) showed a significant increase in mean and total SC from 2013 to 2023 (0.04, 107.26). However, the increases in SC from RFTF, RFTG, returning farmland to unutilized land (RFTU), and CGTF were lower than those in the 2000–2013 period.

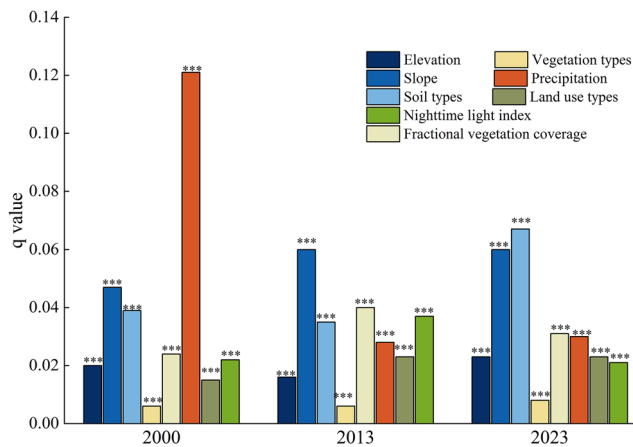


**Fig. 9 | Statistics of q value for driving factors of SC. \*\*\* indicates  $p$  value < 0.001.**

### Quantitative identification of dominant factors for SC

To clarify the driving mechanisms of SC in Guizhou Province, this study employed the Geographical Detector model and its Factor Detector module to quantitatively identify the dominant factors influencing the spatial distribution of SC (Fig. 9). In 2000, precipitation was the dominant factor explaining the spatial distribution of SC ( $q = 0.121$ ), with slope ( $q = 0.047$ ) and soil types ( $q = 0.039$ ) ranking as the second and third dominant factors, respectively. In 2013, the slope exhibited the highest explanatory power ( $q = 0.060$ ), while fractional vegetation coverage (FVC) ( $q = 0.040$ ) and the nighttime light index (NLI) ( $q = 0.037$ ) ranked as the second and third dominant factors, respectively. In 2023, soil types exhibited the strongest explanatory power ( $q = 0.067$ ), slope ( $q = 0.060$ ), and FVC ( $q = 0.031$ ) ranked the second and third dominant factors, respectively. These results indicate that the dominant factors of SC in Guizhou Province exhibited distinct temporal differences.

### Discussion

The surrogate biophysical model adopted in this study was used to assess the relative capacity of SC in the study area and was mainly intended to reveal the relative spatiotemporal ranking of SC supply capacity. Given that the model outputs are dimensionless relative values, this study conducted consistency and reasonableness analysis by comparing the results of the surrogate biophysical method with those of relevant studies using the RUSLE model, focusing on the consistency of spatiotemporal patterns of SC. Niu and Shao<sup>53</sup>, Qiu et al.<sup>54</sup>, Peng et al.<sup>55</sup>, and Fang et al.<sup>29</sup> employed the RUSLE model to analyze the spatial distribution of SC and soil erosion in Guizhou province. They found that the SC capacity of Guizhou Province showed an increasing trend, and it was greater in the southern region compared with the northern and western regions, while soil erosion was more pronounced in the western region. These findings are similar to the spatial distribution pattern of SC derived from the surrogate model based on NPP in this study (Fig. 5). Based on the available evidence, the surrogate biophysical method developed in this study appears ecologically meaningful and operationally feasible, and has the potential to support rapid quantitative assessment and monitoring of ecosystems at large spatial scales.

Previous studies have demonstrated that increasing vegetation coverage can be an effective measure for enhancing SC services in karst areas<sup>19,26</sup>. In this study, results showed that the strongest SC area in Guizhou Province is situated in the southern region, which is primarily composed of non-karst terrains and elevated depressions, harboring forest ecosystems with minimal human disturbance and a relatively pristine ecological environment. Consequently, the southern part of Guizhou province exhibits higher SC compared to other areas. Conversely, the weakest SC area was found in the northern and western parts, characterized by their karstic canyons and plateaus with significant soil erosion issues. Our study found that the SC capacity of forests was highest among all land use types. This confirms that the capacity of SC is influenced by the type of vegetation and the amount of

vegetation cover, and will consequently change with the age of the ecosystem and the environmental factors present<sup>42</sup>.

We found that the 8–15° slope region in Guizhou province had a greater SC capacity compared with steep-slope areas, with SC decreasing steadily as slope steepness increased (Fig. 7); this aligns with the results reported by Zhu et al.<sup>56</sup>, Wang et al.<sup>57</sup>, and Xiao et al.<sup>58</sup>. Because slope is a fundamental factor determining runoff washout capacity, a gentler slope results in a reduced runoff flow rate and increased SC capacity<sup>59</sup>. Our study found that the SC capacity was strongest at 500–1000 m altitude and decreased as altitude increased (Fig. 7), which is consistent with the results of Rao et al.<sup>60</sup> and An et al.<sup>61</sup>. Under high-elevation, fragile environmental conditions, soil erosion is severe due to the interaction of increased precipitation and low vegetation cover, resulting in a decline in SC capacity<sup>62,63</sup>. The high-altitude areas on the Guizhou Plateau are dominated by karst mountains and plateau surfaces, characterized by a fragile ecological environment and severe soil erosion. In addition, overgrazing of grasslands in this region leads to a low vegetation coverage rate, which is the primary cause for the decline in SC capacity. The average annual precipitation in Guizhou Province shows similar spatial distribution characteristics to SC (Figs. 5 and 10). The study revealed that SC first increased and then gradually decreased with increasing precipitation (Fig. 7), aligning with the conclusions drawn by Niu and Shao<sup>53</sup>. The SC capacity declined when precipitation was less than 1000 mm. This is probably because lower precipitation increased soil moisture stress, which is not conducive to vegetation growth and therefore hinders the improvement of SC capacity, while excessive precipitation can exacerbate surface erosion caused by runoff<sup>59</sup>. During the study period, the status of rocky desertification in Guizhou Province has undergone a continuous improvement (Fig. 10). Previous research has demonstrated that the higher the degree of rocky desertification in an area, the higher the rate of soil erosion<sup>64</sup>. Surprisingly, the SC in LKRD was found to be higher than that in PKRD in this study (Fig. 7). We hypothesize that the reason for this difference could be attributed to the prevalence of wastelands and sloping cultivated lands in PKRD, which experience significant soil erosion, compared to LKRD, where soil erosion is minimal. This highlights the need to prioritize management efforts in PKRD, including initiatives like slope conversion and afforestation.

Ecological engineering has had a notable impact on regional ecology by altering land use, resulting in changes in vegetation cover, decreased soil erosion, and substantial enhancements in soil carbon storage<sup>65,66</sup>. In this study, SC was enhanced from 2000 to 2023 through various ecological restoration measures, which aligns with the results of Zhang et al.<sup>67</sup> and Tan et al.<sup>1</sup>. Results showed that the main measures varied during different time periods, and the primary contributors to SC improvement in Guizhou province were ecological restoration measures involving RFTF from 2000 to 2023 (Table 8), which is consistent with the findings of Qiu et al.<sup>68</sup>. It has also been proposed that the introduction of the Grain for Green Program (GFGP) in Southwest China in 2000 has expanded forest cover, which boosted vegetation coverage and regional environmental conditions, thereby enhancing SC capacity<sup>69</sup>. Besides, further analysis of changes in mean SC values across various ecological measures revealed that the highest mean SC improvement was observed in the RFTW from 2013 to 2023 (Table 8). The construction of numerous hydropower stations in Guizhou province following the West-East Electricity Transmission Project has led to a substantial expansion of its water area, contributing significantly to the increase in SC capacity<sup>70</sup>. This is further verified by the findings of this study.

Earlier studies have indicated that implementing ecological projects facilitates rural-urban labor migration<sup>71</sup>, which could potentially mitigate the adverse effects of population growth on ecological restoration. Nevertheless, the process of urbanization can contribute to environmental pollution and the excessive and unsustainable use of natural resources<sup>72–74</sup>. The conversion of farmland to construction land between 2000 and 2013 led to a decrease in SC (Table 8). This highlights the negative effects of urbanization. Therefore, it is necessary to take measures to balance the relationship between urbanization and soil conservation. Specifically, this involves optimizing the territorial spatial pattern of land use and protection based on

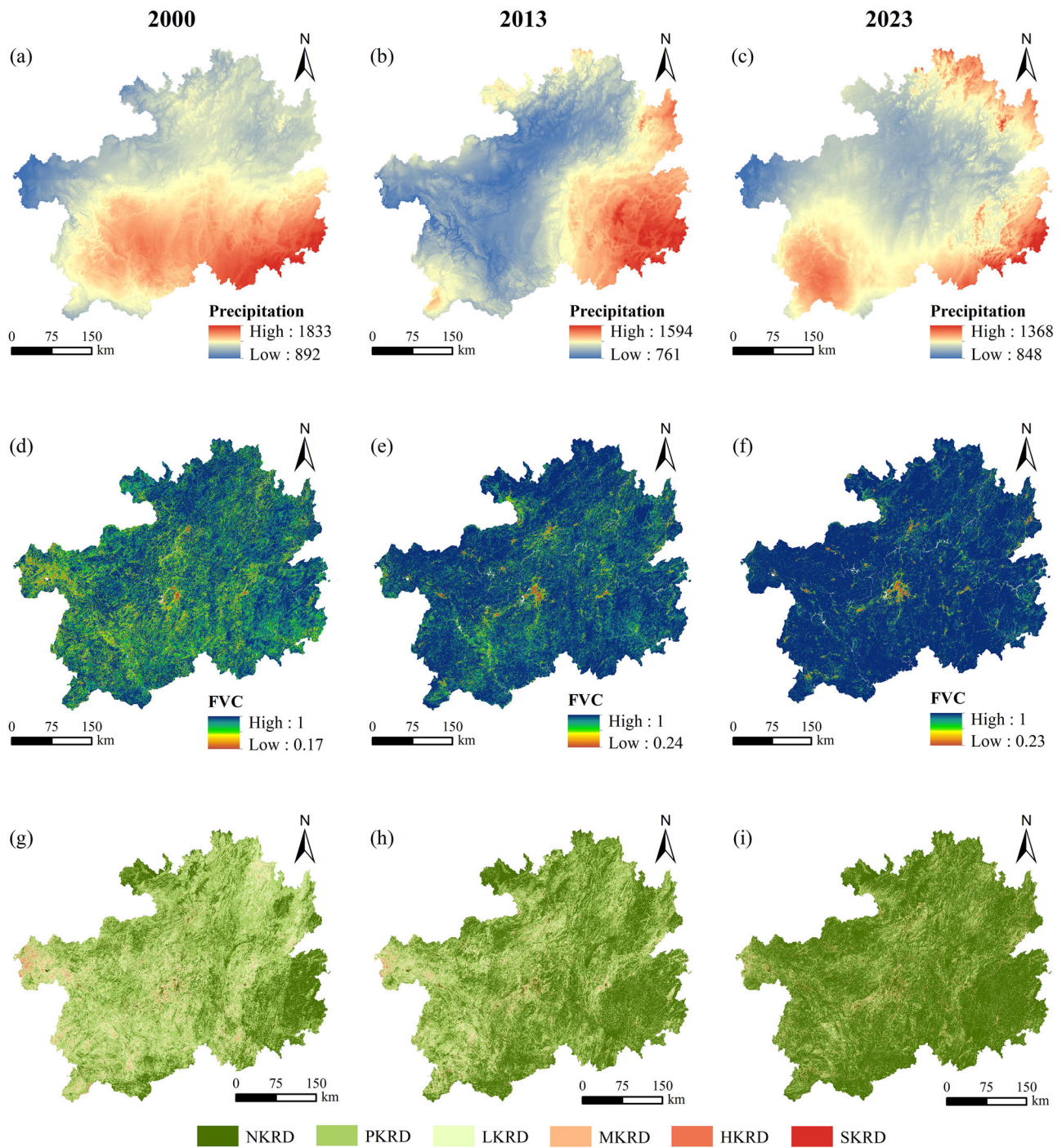


**Fig. 10 | Spatial distribution of precipitation, FVC, and rocky desertification degree in Guizhou province. a–c** Precipitation (2000, 2013, 2023); **d–f** FVC (2000, 2013, 2023); **g–i** Rocky desertification degree (2000, 2013, 2023).

the spatial pattern of SC, thereby minimizing the encroachment of urbanization on areas with high SC capacity. For regions already subjected to urbanization-induced disturbances, ecological restoration measures such as ecological slope protection and vegetation reconstruction should be adopted to enhance the resilience of SC services. In addition, priority should be given to the development of low-disturbance industries such as ecotourism to reduce excessive dependence on the ecosystem. This study also discovered that the overall improvement in SC under various ecological restoration methods in the later period was not as effective as that in the earlier period. This was primarily due to the introduction of the “compensation balance for agricultural land acquisition” (RCBF) policy<sup>75</sup>. This initiative has caused a notable conversion of ecological land (forests, grasslands, and water bodies)

to farmland, leading to a substantial reduction in SC. This reduction largely offsets the benefits gained from other ecological restoration efforts.

Although ecological restoration policies have achieved remarkable results in promoting vegetation growth and enhancing SC in karst regions, it is inadvisable to focus solely on increasing forest and grassland coverage. This research discovered that forests have the highest SC capacity, but simply focusing on SC capacity within one type of land use is insufficient, and in-depth analyses of SC capacity changes during the conversion between different land use types are needed to propose suitable restoration strategies that align with the specific ecological requirements and geographical features of the region. This study found that the RFTW measure can effectively improve SC in karst areas. It suggests focusing on transforming farmland into water bodies rather than

solely returning farmland to grasslands and forests. This forms the foundation for tailoring land use policies to specific local conditions. However, the karst landform induces a scarcity of surface water, which further exacerbates the issue of engineering water shortages. Coupled with the seasonal variability of precipitation, these factors impose constraints stemming from insufficient water supply on the RFTW Project. Meanwhile, the implementation of this project may lead to the loss of agricultural land and disturbances to hydrological processes, specifically characterized by altered runoff patterns and imbalanced groundwater recharge dynamics. To address these challenges, a comprehensive strategy should be adopted, such as improving water-saving infrastructure, optimizing water resource allocation, and establishing a balanced ecological compensation mechanism to coordinate the relationship between ecological restoration and socio-economic development in karst areas.

The results demonstrate that the dominant driving factors of SC in Guizhou Province exhibited temporal variation over the period 2000–2023. During the study period, slope consistently ranked among the top two dominant factors, which is highly consistent with the provincial regional background with its extensive karst landforms and significant topographic relief. Slope directly affects the scouring intensity of surface runoff and the rate of soil erosion, acting as an inherent and fundamental restrictive factor for the spatial differentiation of SC in karst areas<sup>41,76</sup>. FVC was not a core driving factor in 2000 but emerged as one in 2013 and 2023. This shift may be linked to the advancement of karst desertification control, ecological restoration, and other related projects in Guizhou Province. Vegetation coverage has been continuously improved (Fig. 10), and FVC has become an important regulatory driving factor for SC. In addition, the nighttime light index (NLI) became the third dominant factor in 2013, indicating that human disturbance activities such as urbanization and agricultural production exerted a significant influence on the spatial distribution of SC during this period. On the other hand, soil types emerged as the primary factor in 2023, which may be attributed to the phased regulation of climatic and topographic factors and the sustained improvement in vegetation coverage, leading to the increasingly prominent effects of soil attributes (including soil texture, erosion resistance, and soil layer thickness) on SC<sup>24</sup>. In summary, the evolution of the driving mechanisms for SC in Guizhou Province is not only affected by the phased characteristics of regional natural environmental factors but also closely associated with the spatiotemporal changes in ecological governance and the intensity of human activities.

This study takes Guizhou Province as the research object to explore the impact of ecological restoration projects on the spatio-temporal evolution of SC service, which has significant guiding significance for the formulation and adjustment of ecological restoration policies in karst desertification areas. However, the current research area is limited to Guizhou Province, which, to some extent, restricts the application scope of the research results. In the future, the research scope needs to be expanded to explore the spatio-temporal evolution pattern of SC services across the entire karst areas of southern China. Although the surrogate biophysical model can rapidly characterize the spatiotemporal pattern of SC across Guizhou Province, its oversimplification of biological mechanisms, inadequate consideration of unique karst habitats, and inherent uncertainty in key parameters may lead to deviations in the results. Future research should incorporate additional vegetation functional traits and key karst-specific parameters (e.g., karst topographic attributes and soil properties) into the model, and simultaneously use long-term in-situ monitoring data to conduct model validation and calibration, so as to improve its application accuracy and reliability in karst regions. This study only took into account some natural factors (land use, slope, altitude, rainfall, rocky desertification grade, and vegetation coverage). In the future, big data should be integrated to comprehensively consider natural and socio-economic factors and deeply explore the driving mechanisms of the spatio-temporal evolution of SC services. Furthermore, the current study solely examines how ecological restoration efforts affect SC without thoroughly exploring the trade-off and synergy relationships between the ESs it brings. In the future, we need to delve deeply into the impact of ecological restoration measures on the spatio-temporal distribution of multiple ESs, further optimize the simulation of ecosystem service

models, and adopt a combination of qualitative and quantitative methods to reveal the trade-off synergy and driving mechanisms among them, so as to promote the synergistic enhancement of ecosystem services in karst areas.

In this study, the surrogate biophysical method was adopted to explore the spatio-temporal evolution of SC in Guizhou Province. The results indicated that the SC capacity of Guizhou Province showed an increasing trend from 2000 to 2023. Overall, the spatial pattern of SC was high in the southern region and low in the northwestern and northern regions. SC hotspots were primarily spatially aggregated in Qianxinan and Qiannan, while the coldspots were mainly distributed in the western and northern parts of Guizhou Province. Forests exhibited the highest mean SC values (0.20–0.26). The SC capacity in the LKRD area (0.22) was higher than that in the PKRD area (0.17). RFTF, RFTG, and CGTF were identified as the most effective measures for enhancing SC, contributing to over 94% of the overall improvement in SC capacity. In addition, we found that RFTW became increasingly effective in enhancing SC from 2013 to 2023, with an improvement of 0.04 compared with the previous period (0.01). We therefore conclude that RFTW is a potent strategy for further facilitating karst desertification control. The dominant driving factors of SC exhibited temporal variability, with precipitation, slope, and soil types serving as the key dominant factors of SC in Guizhou Province throughout the study period. Furthermore, it is essential to comprehensively consider the SC capacity under different environmental conditions, to identify and address existing gaps based on this analysis, so as to further clarify the suitability of land use allocation in karst areas. This study quantified the effectiveness of ERPs in karst areas and provided novel optimization directions for karst desertification control. The soil conservation hotspots and priority areas identified in this study cover the entire territory of Guizhou Province, including its karst World Heritage sites. These findings allow for the spatially explicit identification of ecologically critical and vulnerable zones within the heritage sites, providing a scientific basis for ecological restoration, soil and water conservation, and coordinated conservation management. This contributes to maintaining the integrity and authenticity of heritage values while advancing the sustainable development of the regional ecology.

### Data availability

The datasets generated and analyzed during the current study are not publicly available due to data privacy and institutional policy restrictions, but are available from the corresponding author on reasonable request.

Received: 22 November 2025; Accepted: 18 March 2026;

Published online: 01 April 2026

### References

1. Tan, Z. et al. The response and simulation of ecosystem services value to land use/land cover in an oasis, Northwest China. *Ecol. Indic.* **118**, 106711 (2020).
2. Sun, X., Ma, Q. & Fang, G. J. Spatial scaling of land use/land cover and ecosystem services across urban hierarchical levels: patterns and relationships. *Landsc. Ecol.* **38**, 753–777 (2023).
3. Wang, D. J., Shen, Y. X., Li, Y. H. & Huang, J. Rock outcrops redistribute organic carbon and nutrients to nearby soil patches in three karst ecosystems in SW China. *PLoS ONE* **11**, e0160773 (2016).
4. Zhao, H. et al. Dynamic soil erosion in response to LULC changes in mountainous areas of southwest China over the last 40 years: a case study of the Erhai Basin in Yunnan province. *Environ. Sustain. Indic.* **27**, 100755 (2025).
5. Weissert, L. F., Salmund, J. A. & Schwendenmann, L. Photosynthetic CO<sub>2</sub> uptake and carbon sequestration potential of deciduous and evergreen tree species in an urban environment. *Urban Ecosyst.* **20**, 663–674 (2017).
6. Peng, J. et al. Simulating the impact of Grain-for-Green Programme on ecosystem services trade-offs in Northwestern Yunnan, China. *Ecosyst. Serv.* **39**, 100998 (2019).

7. Liu, W. C., Liu, J. Y. & Kuang, W. H. Spatio-temporal characteristics of soil protection efforts of the grain for green project in northern Shaanxi province. *J. Geogr. Sci.* **30**, 401–422 (2020).
8. He, J. Institutional bricolage in payment for ecosystem services: insights from the Sloping Land Conversion Programme in upland communities, Southwest China. *Asia Pac. Viewp.* **62**, 164–178 (2021).
9. Liu, Y., Zhao, W. W. & Jia, L. Z. Soil conservation service: concept, assessment, and outlook. *Acta Ecol. Sin.* **39**, 432–440 (2019).
10. Kong, L. Q. et al. Evaluating indirect and direct effects of eco-restoration policy on soil conservation service in Yangtze River Basin. *Sci. Total Environ.* **631–632**, 887–894 (2018).
11. Guo, X. J., Shao, Q. Q. & Luo, Y. Effects of different management measures on soil conservation and the influence of environmental conditions: a case study involving UAV remote sensing on the Loess Plateau. *Remote Sens. Ecol. Conserv.* **8**, 683–697 (2022).
12. He, C., Xiong, K. N. & Rong, L. Trade-offs and synergies of ecosystem services and their drivers in the forests of the South China Karst. *npj Herit. Sci.* **13**, 298 (2025).
13. Ford, D., & Williams, P. D. *Karst Hydrogeology and Geomorphology* (John Wiley & Sons, 2007).
14. Chen, Q. W., Lu, S. X., Xiong, K. N. & Zhao, R. Coupling analysis on ecological environment fragility and poverty in South China Karst. *Environ. Res.* **201**, 111650 (2021).
15. Jiang, Z. C., Lian, Y. Q. & Qin, X. Q. Rocky desertification in Southwest China: impacts, causes, and restoration. *Earth-Sci. Rev.* **132**, 1–12 (2014).
16. Jing, J., Li, R., Xiao, L. L., Shu, D. C. & Yang, P. P. Interpreting and modelling the daily extreme sediment events in karst mountain watersheds. *Sci. Total Environ.* **926**, 171956 (2024).
17. Tong, X. W. et al. Increased vegetation growth and carbon stock in China karst via ecological engineering. *Nat. Sustain.* **1**, 44–50 (2018).
18. Yue, Y. M. et al. Large scale reforestation of farmlands on sloping hills in South China karst. *Landsc. Ecol.* **35**, 1445–1458 (2020).
19. Chen, Y., Cheng, C., Xiong, K. N., Rong, L. & Zhang, S. H. Quantifying the biodiversity and ecosystem service outcomes of karst ecological restoration: a meta-analysis of South China Karst. *CATENA* **245**, 108278 (2024).
20. Liu, Y. F., Liu, Y., Shi, Z. H., López-Vicente, M. & Wu, G. L. Effectiveness of re-vegetated forest and grassland on soil erosion control in the semi-arid Loess Plateau. *CATENA* **195**, 104787 (2020).
21. Zhang, D. et al. Trade-offs and synergistic evolution of ecosystem services and land use driving mechanisms in karst ecologically vulnerable areas of China. *Geocarto Int.* **40**, 2509111 (2025).
22. Zhou, B., Chen, G. P., Yu, H. R., Zhao, J. S., & Yin, Y. “Revealing the Nonlinear Impact of Human Activities and Climate Change on Ecosystem Services in the Karst Region of Southeastern Yunnan Using the XGBoost–SHAP Model.” *Forests* **15**, 1420 (2024).
23. Qu, S. et al. Spatial-temporal evolution and driving factors of ecosystem services trade-offs and synergies in karst areas from a geospatial perspective. *Land Degrad. Dev.* **35**, 3448–3460 (2024).
24. Li, J. W. et al. Matching and driving mechanism analysis of the supply and demand relationships of soil conservation services in karst peak-cluster depression basin in Southwest Guangxi, China. *CATENA* **246**, 108438 (2024).
25. Tang, Z. Y. & Li, R. Small watersheds are the best control and management unit for improving soil conservation services in karst areas. *Sci. Total Environ.* **953**, 176162 (2024).
26. Chen, Y., Xiong, K. N., Luo, L., Zhang, S. H. & Chen, J. Y. Trade-offs/synergies and drivers of ecosystem service sustainability at multiple scales: insights from the South China Karst. *Land Degrad. Dev.* <https://doi.org/10.1002/ldr.70021> (2025).
27. Pandey, R., Mehta, D., Kumar, V. & Prakash Pradhan, R. Quantifying soil erosion and soil organic carbon conservation services in indian forests: a RUSLE-SDR and GIS-based assessment. *Ecol. Indic.* **163**, 112086 (2024).
28. Xu, Z., Zhang, S. H., Zhou, Y., Hou, X. N. & Yang, X. Y. Characteristics of watershed dynamic sediment delivery based on improved RUSLE model. *CATENA* **219**, 106602 (2022).
29. Fang, F. Y. et al. RUSLE model evaluation of the soil and water conservation ratio of the Guizhou province in China between 2000 and 2019. *Sustainability* **14**, 8219 (2022).
30. Fu, B. J. et al. Assessing the soil erosion control service of ecosystems change in the Loess Plateau of China. *Ecol. Complex.* **8**, 284–293 (2011).
31. Andrew, M. E., Wulder, M. A., Nelson, T. A. & Coops, N. C. Spatial data, analysis approaches, and information needs for spatial ecosystem service assessments: a review. *GIScience Remote Sens.* **52**, 344–373 (2015).
32. Costanza, R. et al. The value of ecosystem services: putting the issues in perspective. *Ecol. Econ.* **25**, 67–72 (1998).
33. Zurlini, G. et al. Key fundamental aspects for mapping and assessing ecosystem services: predictability of ecosystem service providers at scales from local to global. *Ann. di Bot.* **4**, 53–63 (2014).
34. Odum, H. T. & Odum, E. P. The energetic basis for valuation of ecosystem services. *Ecosystems* **3**, 21–23 (2000).
35. Ingraham, M. W. & Foster, S. G. The value of ecosystem services provided by the U.S. National Wildlife Refuge System in the contiguous U.S. *Ecol. Econ.* **67**, 608–618 (2008).
36. Egoh, B. et al. Mapping ecosystem services for planning and management. *Agric. Ecosyst. Environ.* **127**, 135–140 (2008).
37. Barral, M. P. & Oscar, M. N. Land-use planning based on ecosystem service assessment: a case study in the Southeast Pampas of Argentina. *Agric. Ecosyst. Environ.* **154**, 34–43 (2012).
38. Carreño, L., Frank, F. C. & Viglizzo, E. F. Tradeoffs between economic and ecosystem services in Argentina during 50 years of land-use change. *Agric. Ecosyst. Environ.* **154**, 68–77 (2012).
39. Zhang, L. W. et al. Mapping ecosystem services for China’s ecoregions with a biophysical surrogate approach. *Landsc. Urban Plan.* **161**, 22–31 (2017).
40. Zhang, L. W., Lü, Y. H., Fu, B. J. & Zeng, Y. Uncertainties of two methods in selecting priority areas for protecting soil conservation service at regional scale. *Sustainability* **9**, 1577 (2017).
41. Gao, J. B., Zuo, L. Y. & Liu, W. L. Environmental determinants impacting the spatial heterogeneity of karst ecosystem services in Southwest China. *Land Degrad. Dev.* **32**, 1718–1731 (2021).
42. Zhang, S. H., Xiong, K. N., Qin, Y., Min, X. Y. & Xiao, J. Evolution and determinants of ecosystem services: insights from South China karst. *Ecol. Indic.* **133**, 108437 (2021).
43. Zhang, Z. Y. et al. Variations in erosive rainfall threshold and sediment production between karst and non-karst slopes. *CATENA* **251**, 108820 (2025).
44. Brandt, M. et al. Satellite-observed major greening and biomass increase in south china karst during recent decade. *Earth’s. Future* **6**, 1017–1028 (2018).
45. Xi, H. P. et al. Spatio-temporal characteristics of rocky desertification in typical Karst areas of Southwest China: a case study of Puding County, Guizhou Province. *Acta Ecol. Sin.* **38**, 8919–8933 (2018).
46. Halmy, M. W. A., Gessler, P. E., Hicke, J. A. & Salem, B. B. Land use/land cover change detection and prediction in the north-western coastal desert of Egypt using Markov-CA. *Appl. Geogr.* **63**, 101–112 (2015).
47. Gao, J. B. & Wang, H. Temporal analysis on quantitative attribution of karst soil erosion: a case study of a peak-cluster depression basin in Southwest China. *CATENA* **172**, 369–377 (2019).
48. Potter, C. S. et al. Terrestrial ecosystem production: a process model based on global satellite and surface data. *Glob. Biogeochem. Cycles* **7**, 811–841 (1993).
49. Sharpley, A. N. & Williams, J. R. (eds). EPIC-erosion/productivity impact calculator: 1. Model documentation. 235-pp (1990).
50. Zhang, Z. M., Huang, X. F. & Zhou, Y. C. Factors influencing the evolution of human-driven rocky desertification in karst areas. *Land Degrad. Dev.* **32**, 817–829 (2021).

51. Wang, J. F. & Xu, C. D. Geodetector: principle and prospective. *Acta Geogr. Sin.* **72**, 116–134 (2017).
52. Wang, J. F., Zhang, T. L. & Fu, B. J. A measure of spatial stratified heterogeneity. *Ecol. Indic.* **67**, 250–256 (2016).
53. Niu, L. N. & Shao, Q. Q. Soil conservation service spatiotemporal variability and its driving mechanism on the Guizhou plateau, China. *Remote Sens.* **12**, 2187 (2020).
54. Qiu, S. J. et al. Understanding the relationships between ecosystem services and associated social-ecological drivers in a karst region: a case study of Guizhou Province, China. *Prog. Phys. Geogr. Earth Environ.* **45**, 98–114 (2021).
55. Peng, J. et al. Distinguishing the impacts of land use and climate change on ecosystem services in a karst landscape in China. *Ecosyst. Serv.* **46**, 101199 (2020).
56. Zhu, M. Y. et al. Spatial and temporal characteristics of soil conservation service in the area of the upper and middle of the Yellow River, China. *Heliyon* **5**, <https://doi.org/10.1016/j.heliyon.2019.e02985> (2019).
57. Wang, S. et al. Analysis on trend evolution and driving factors of soil protection services in eastern sandy region of China. *Ecol. Indic.* **154**, 110816 (2023).
58. Xiao, Q., Xiao, Y. & Tan, H. Changes to soil conservation in the Three Gorges Reservoir Area between 1982 and 2015. *Environ. Monit. Assess.* **192**, 44 (2019).
59. Lu, R. R., Dai, E. F. & Wu, C. S. Spatial and temporal evolution characteristics and driving factors of soil conservation services on the Qinghai-Tibet Plateau. *CATENA* **221**, 106766 (2023).
60. Rao, E., Ouyang, Z., Yu, X. & Xiao, Y. Spatial patterns and impacts of soil conservation service in China. *Geomorphology* **207**, 64–70 (2014).
61. An, Y. M., Zhao, W. W., Li, C. J. & Sofia Santos Ferreira, C. Temporal changes on soil conservation services in large basins across the world. *CATENA* **209**, 105793 (2022).
62. Wang, Y. B., Niu, F. J., Wu, Q. B. & Gao, Z. Y. Assessing soil erosion and control factors by radiometric technique in the source region of the Yellow River, Tibetan Plateau. *Quat. Res.* **81**, 538–544 (2014).
63. Amanollahi, J., Gharibi, S. & Rastkhadiv, A. Prediction of soil erosion control ecosystem service using machine learning based on the ANN model in Asia. *Environ. Sustain. Indic.* **26**, 100723 (2025).
64. Chen, P. & Lian, Y. Q. Modeling of soil loss and its impact factors in the Guijiang Karst River Basin in Southern China. *Environ. Earth Sci.* **75**, 352 (2016).
65. Li, Y. W. et al. Trade-off analyses between food provision and soil conservation service of Grain for Green Program in Mountainous Area. *Int. Soil Water Conserv. Res.* **12**, 43–53 (2024).
66. Wang, X. F. et al. Soil conservation on the Loess Plateau and the regional effect: impact of the ‘Grain for Green’ Project. *Earth Environ. Sci. Trans. R. Soc. Edinb.* **109**, 461–471 (2018).
67. Zhang, Y. Q., Zhao, X., Gong, J., Luo, F. & Pan, Y. P. Effectiveness and driving mechanism of ecological restoration efforts in China from 2009 to 2019. *Sci. Total Environ.* **910**, 168676 (2024).
68. Qiu, S. J., Peng, J., Zheng, H. N., Xu, Z. H. & Meersmans, J. How can massive ecological restoration programs interplay with social-ecological systems? A review of research in the South China karst region. *Sci. Total Environ.* **807**, 150723 (2022).
69. Hu, Z. Y. et al. Changes in ecosystem service values in karst areas of China. *Agric. Ecosyst. Environ.* **301**, 107026 (2020).
70. Zhu, Y. N. et al. Water transfer and losses embodied in the West–East electricity transmission project in China. *Appl. Energy* **275**, 115152 (2020).
71. Liu, J. G., Li, S. X., Ouyang, Z. Y., Tam, C. & Chen, X. D. Ecological and socioeconomic effects of China’s policies for ecosystem services. *Proc. Natl. Acad. Sci. USA* **105**, 9477–9482 (2008).
72. Hu, X. S. et al. Geographic variations of ecosystem service intensity in Fuzhou City, China. *Sci. Total Environ.* **512–513**, 215–226 (2015).
73. Peng, J. et al. Ecosystem services response to urbanization in metropolitan areas: thresholds identification. *Sci. Total Environ.* **607–608**, 706–714 (2017).
74. Xu, S. N., Liu, Y. F., Wang, X. & Zhang, G. X. Scale effect on spatial patterns of ecosystem services and associations among them in semi-arid area: a case study in Ningxia Hui Autonomous Region, China. *Sci. Total Environ.* **598**, 297–306 (2017).
75. Chen, W. X. et al. Analyzing requisition–compensation balance of farmland policy in China through telecoupling: A case study in the middle reaches of Yangtze River Urban Agglomerations. *Land Use Policy* **83**, 134–146 (2019).
76. Gao, J., Jiang, Y. & Anker, Y. Contribution analysis on spatial tradeoff/synergy of Karst soil conservation and water retention for various geomorphological types: Geographical detector application. *Ecol. Indic.* **125**, 107470 (2021).

### Acknowledgements

This research was supported by the China Overseas Expertise Introduction Project for Discipline Innovation (No. D17016), the Major Special Project of Provincial Science and Technology Program of Guizhou Province of China (No.6007 2014 QKHZDZXZ), and the Project of Geographical Society of Guizhou Province (No. 20160101). The authors wish to express their gratitude to who gave kind support and advices but was not included as co-authors, including Qingqing Xie and Qian Zhai for sharing their knowledge on models and software.

### Author contributions

All authors are contributed to the manuscript. Y.M.: Conceptualization, methodology, formal analysis, Software, data curation, writing—original draft. K.X.: Writing—review and editing, funding acquisition. X.Y.: Software, writing—review and editing. G.L.: Supervision. L.C.: Writing—review and editing. All authors have read and approved the final manuscript.

### Competing interests

The authors declare no competing interests. Author Kangning Xiong is Editorial Board Member of npj Heritage Science. Kangning Xiong was not involved in the journal’s review of, or decisions related to, this manuscript.

### Additional information

**Correspondence** and requests for materials should be addressed to Kangning Xiong.

**Reprints and permissions information** is available at <http://www.nature.com/reprints>

**Publisher’s note** Springer Nature remains neutral with regard to jurisdictional claims in published maps and institutional affiliations.

**Open Access** This article is licensed under a Creative Commons Attribution-NonCommercial-NoDerivatives 4.0 International License, which permits any non-commercial use, sharing, distribution and reproduction in any medium or format, as long as you give appropriate credit to the original author(s) and the source, provide a link to the Creative Commons licence, and indicate if you modified the licensed material. You do not have permission under this licence to share adapted material derived from this article or parts of it. The images or other third party material in this article are included in the article’s Creative Commons licence, unless indicated otherwise in a credit line to the material. If material is not included in the article’s Creative Commons licence and your intended use is not permitted by statutory regulation or exceeds the permitted use, you will need to obtain permission directly from the copyright holder. To view a copy of this licence, visit <http://creativecommons.org/licenses/by-nc-nd/4.0/>.

© The Author(s) 2026